Applied Catalysis B: Environmental 323 (2023) 122164

Contents lists available at ScienceDirect

Applied Catalysis B: Environmental

journal homepage: www.elsevier.com/locate/apcatb

Cascade upcycling polystyrene waste into ethylbenzene over Fe_2N @ C

Zhukun Zhang [a,b], Dongxian Li [a,b], Jia Wang [a,b,*], Jianchun Jiang [a,b,*]

[a] Jiangsu co-Innovation Center for Efficient Processing and Utilization of Forest Resources, International Innovation Center for Forest Chemicals and Materials, College of Chemical Engineering, Nanjing Forestry University, Longpan Road 159, Nanjing 210037, China
[b] Jiangsu Province Key Laboratory of Biomass Energy and Materials, Institute of Chemical Industry of Forest Products, Chinese Academy of Forestry (CAF), No. 16, Suojin Five Village, Nanjing 210042, China

ARTICLE INFO

Keywords:
Hydropyrolysis
Hydrocracking
Polystyrene
Iron nitride
Ethylbenzene

ABSTRACT

Thermochemical conversion is one of the most effective ways to upcycle organic solid wastes into fuels and/or value-added chemicals. In this study, the tandem hydropyrolysis/hydrocracking of polystyrene (PS) to produce ethylbenzene was studied using metal nitrides as catalysts. Fe, N co-doped carbon-based catalyst (Fe_2N @ C) with core-shell structure was synthesized. The experimental results showed that carbon doping significantly improved the catalytic performance of iron nitride. The yield of ethylbenzene obtained from Fe_2N @ C catalysis was 81 wt %, which is much higher than that of Fe_2N (63.3 wt%) and commercial iron nitride (FeN, 4.9 wt%) under the hydropyrolysis temperature of 480 ℃, hydrocracking temperature of 280 ℃, and low H_2 pressure of 0.2 MPa. The high catalytic activity of Fe_2N @ C is ascribed to the synergy of metal-based selective hydrogenation and acid site-mediated C-C bond activation. This work provides a flexible and efficient catalytic technology for the high-value utilization of polystyrene waste.

1. Introduction

Plastics have become a necessity of the modern life due to the low production cost, low density, and high durability [1]. Global plastic production rose from 322 million tons in 2015–348 million tons in 2017, with global demand expected to quadruple by 2050 [2]. Polystyrene (PS) accounts for 7% of global plastic consumption and is widely used in food packaging, electrical appliances, construction, medical, and toys [3–6]. The vast applications and continuous demand for plastics caused the accumulation of plastic waste. Incineration, landfills, mechanical recycling, and chemical recycling are the main strategies to deal with plastic waste [7]. However, incineration can produce many toxic and harmful substances, such as dioxins, polycyclic aromatic hydrocarbons, etc., which have serious impacts on human health and environment [6,8,9]. Plastics are difficult to degrade naturally, and landfills caused its accumulation which takes up a lot of space. Furthermore, marine plastic pollution has effected more than 200 species globally due to ingestion, starvation, and suffocation [10]. Plastics are petro-derived products and have the potential to produce liquid fuels and/or higher value-added chemicals [11]. It is projected that in 2040 the global energy consumption was estimated to be 17.5 thousand Mtoe (Million tons of oil equivalent, Mtoe) [10]. To address the issues of plastic pollution and high energy demand, the conversion of plastic waste to valuable alternative fuels would be an ideal option [10]. Thermochemical conversion is a technically feasible method to convert solid waste into gaseous/liquid fuels or high value-added chemicals through pyrolysis, gasification, liquefaction or combustion [12].

Regarding the thermochemical conversion of plastic waste, pyrolysis has been highlighted for decades. Fast pyrolysis is the process of converting polymers into initial monomers or oligomers through heat in the absence of oxygen [3]. Notably, the short residence times (0.5–2 s), rapid heating rate, and moderate temperatures (400–650 ℃) required for fast pyrolysis of plastic waste has attracted considerable research interest [3,6,12–14]. For example, at rapid heating rate of 10–200 ℃/s, the fast pyrolysis of plastic yields 37–95 wt% liquid oil [15]. The pyrolysis of polystyrene yielded 78.7% of monomeric styrene at the pyrolysis temperature of 600 °C in a fluidized-bed reactor [16]. However, the products of fast pyrolysis polystyrene are dominated with highly unsaturated styrene [17–20]. From the perspective of drop-in liquid fuels, the presence of unsaturated styrene makes the poor stability of liquid oil, indicating that further hydrotreatment of styrene is necessary. It is worthy noting that hydrofining is an efficient approach to improve

* Corresponding authors at: Jiangsu co-Innovation Center for Efficient Processing and Utilization of Forest Resources, International Innovation Center for Forest Chemicals and Materials, College of Chemical Engineering, Nanjing Forestry University, Longpan Road 159, Nanjing 210037, China.
E-mail addresses: wangjia@njfu.edu.cn (J. Wang), jiangjc@caf.ac.cn (J. Jiang).

https://doi.org/10.1016/j.apcatb.2022.122164
Received 18 September 2022; Received in revised form 4 November 2022; Accepted 9 November 2022
Available online 11 November 2022

the stability of liquid products attained from plastic pyrolysis. Therefore, further hydrogenation/hydrocracking of styrene-based intermediates into high-value liquid fuel ethylbenzene is an ideal treatment option.

Recently, the hydrocracking of plastic wastes over bifunctional metal-based catalysts has been highlighted [21–26]. Hydrocracking is the conversion of polymers to smaller molecules in the presence of hydrogen, and the simultaneous or successive hydrogenation of unsaturated molecules generated during the cracking process [27]. For instance, PS hydrogenolysis over a Ru/Nb_2O_5 catalyst at 300 ℃ under 5 bar H_2 pressure for 16 h in octane yielded 75.9% total monocyclic arenes, 65% benzene, 11% ethylbenzene [28]. However, the long reaction times (>10 h) and high pressure (5–30 bar) limit the application of hydrocracking [29–32]. The development of highly efficient catalytic technologies is an effective way to rationally upcycle plastics. In light of these facts, a two-step process combining fast pyrolysis of plastic waste followed by hydrocracking of produced intermediates was proposed in this study. This process enables to tune the quality of the liquid hydrocarbons by selecting suitable catalysts and operating conditions in the presence of hydrogen [33–35].

Bifunctional metal-based catalysts are an important class for hydrocracking that combine metal phase (e.g., Pt, Ru, Pd, Au) to capture and dissociate hydrogen molecules, and acidic supports (e.g., zeolites, silicon-alumina oxides, sulfated zirconia) to promote the depolymerization of plastic waste [21–24,33,36,37]. In particular, Pt/zeolites were a kind of commonly used catalysts for the hydrocracking of plastic waste. However, the small pore size of zeolites prevents large molecules from entering the interior of the pore channel, and the high price of precious metals limits their practical application potential [38]. Transition metal nitride is an intermetallic compound. Due to its special bonding, intermetallic compounds have different electronic and geometric structures on the surface, and there are a lot of dislocations and defects in the bulk phase, which can effectively modulate the bonding between the surface and the adsorbed molecules (substrates, intermediates, target products), exhibiting similar properties to noble metal catalyst [39–42]. Specially, transition metal (Fe, Co, Ni, etc.) and nitrogen co-doped carbon-based catalysts are considered as good substitutes for Pt-based catalysts [43–45]. In particular, Fe-based catalyst have reasonable price and abundant source [46]. Consequently, we synthesized a Fe-based nitrides catalyst with core-shell structure for the two-step pyrolysis-catalytic hydrocracking of polystyrene. The protective carbon shell can buffer serious volume change, prevent the agglomeration of Fe_2N particles, and protect the air-sensitive Fe_2N from oxidation [47]. The iron nitride performance is modified by the insertion of carbon atoms, which can provide a significant redistribution of electron density, and making the carbon materials is tuned from inert to active [48].

Here, we synthesized a Fe, N co-doped carbon-based catalyst (Fe_2N @ C) with core-shell structure. The crystal structure, surface property, and acid properties of as-prepared Fe_2N @ C catalyst were studied at first. Then, the catalytic degradation of polystyrene over Fe_2N @ C catalyst was investigated in a two-step pressurized flow-through fixed-bed reactor. The effect of Fe_2N @ C catalyst on the thermal degradation of polystyrene plastics was studied. We found that the Fe_2N @ C showed high activity in converting PS plastic into ethylbenzene. Meanwhile, the formation of ethylbenzene was promoted by adjusting the catalyst loading and optimizing reaction conditions. Thirdly, the yield of ethylbenzene over commercial metal nitrides (TaN, Cr_2N, NNb, GdN, and FeN) catalysis was compared. Fe-based nitrides exhibit better catalytic performance. Finally, a further comparative analysis of the effects of FeN, pure Fe_2N, and as-prepared Fe_2N @ C catalysts on generating ethylbenzene from polystyrene was performed. A possible reaction pathway for the degradation of polystyrene to ethylbenzene was proposed.

2. Experiment

2.1. Materials and chemicals

Polystyrene (average Mw 35,000, was pulverized to 60 mesh) was obtained from the Sigma-Aldrich Corporation, Shanghai, China. Iron (III) chloride ($FeCl_3$, AR), and sodium hydroxide (NaOH, AR, 96%) were purchased from Macklin Chemical Reagent company, Shanghai, China. Tris(hydroxymethyl)methyl aminomethane ($C_4H_{11}NO_3$, ACS, ≥99.8%), dopamine hydrochloride ($C_8H_{12}ClNO_2$, 98%) were provided by Aladdin, Shanghai, China. Chromium nitride (Cr_2N), niobium nitride (NNb), tantalum nitride (metals basis, 99.5%, TaN), gadolinium (III) nitride (REO, 99.5%, GdN), iron nitride (Marked as FeN) purchased from Alfa Aesar, Shanghai, China. Hydrochloric acid (HCl, AR) and ethanol absolute were provided by Sinopharm Chemical Reagent, Shanghai, China. All reagents were not purified before use.

2.2. Catalyst preparation

2.2.1. Synthesis of Fe_2O_3 nanocubes

The typical synthesis method of Fe_2O_3 is hydrothermal precipitation [49]. 50 ml 5.4 M NaOH solution was added to 50 ml 2 M $FeCl_3$ solution under continuous stirring at 75 °C. After the solution is mixed, continue stirring for 5 min under the same conditions. The resultant $Fe(OH)_3$ gel was transferred to a 100 ml autoclave and placed in an oven at 100 °C for 4 days. After the temperature dropped to room temperature, the solid was collected by filtration. The sample was washed with deionized water and absolute ethanol several times and placed in a vacuum drying oven at 60 °C overnight.

2.2.2. Synthesis of Fe_2N @ C yolk-shell nanocubes

Fe_2N @ C was prepared by self-polymerization of dopamine [50]. 120 mg Fe_2O_3 nanocubes were dispersed in 100 ml of Tris-HCl (Tri (Hydroxymethyl)Amino Methane Hydrochloride) buffer solution (pH=8.5, 10 Mm) by sonication for 30 min, subsequently, 70 mg dopamine hydrochloride was added into the above solution and ultrasonic treatment was continued for 5 min. The above mixture was subjected to continuous magnetic stirring at room temperature for 24 h. The resultant product was collected via centrifugation and washed three times with deionized water and absolute ethanol, respectively, and dried at 70 °C overnight under a vacuum. The obtained sample was labeled as Fe_2O_3 @PDA. The as-obtained Fe_2O_3 @PDA nanocubes were loaded in a porcelain boat and annealed at 500 ℃ for 3 h under an atmosphere of NH_3 with a heating rate of 2 ℃/min. The resultant product was denoted Fe_2N @ C, pure Fe_2N was prepared by direct annealing of Fe_2O_3 nanocubes under the same conditions.

2.3. Characterization

Thermogravimetric analysis (TGA) was measured from room temperature to 800 ℃ in N_2 with a heating rate of 10 ℃/min using a thermogravimetric analyzer (NETSCH JUPITER F3, Germany). Field-emission transmission electron microscope (TEM, JEOL-JEM 2100 F, Japan) and EDS mapping were used to analyze microstructure and element distribution. X-ray diffraction (XRD, SmartLab 9 kW, Japan) was used for crystal structure analysis of catalysts. The XRD spectra were determined by a UItima IV diffractometer using CuKα radiation in the range of 2θ from 10° to 80° (10° min^{-1}). X-ray photoelectron spectroscopy (XPS, Thermo Fisher K-Alpha, United States) was used to analyze the elemental composition and valency of the sample surface. The Raman spectra were obtained by a Horiba scientific-LabRAM HR evolution, Japan. The specific surface area and pore size distribution were measured using an adsorption instrument (BELSORP MaxII, MicrotracBEL Japan) with nitrogen at 77 K. Before performing the measurement, the sample was pretreated at 200 °C for 10 h. The ammonia temperature-programmed desorption (NH_3-TPD,

MicrotracBEL Japan) was conducted on a Micromeritics BETCAT-A to obtain the strength and density of acid sites.

2.4. Reaction procedure

The hydropyrolysis-hydrocracking of polystyrene was conducted in a two-step pressurized fixed-bed reactor (RX3050TR, Frontier Laboratories, Japan, Fig. 1) connected with an online gas chromatography-mass spectrometry (GC/MS). Specifically, polystyrene hydropyrolysis was conducted in the 1st reactor, and the produced intermediates (mainly styrene monomer) were vapor-phase hydrocracked in the 2nd reactor. The mass of sample was maintained at 0.3 ± 0.05 mg for each experiment. The catalyst is mixed with quartz sand (50 mg) and loaded into a quartz tube with a length of 78 mm, out diameter of 4 mm, and inner diameter of 3 mm. The catalyst was reduced for 3 h at 400 ℃ in the 2nd reactor before use (was denoted as Fe_2N @ C-H_2). Hydropyrolysis temperature and hydrocracking temperature were kept at 480 ℃ and 280 ℃, respectively. The reaction pressure was maintained at 0.2 MPa. Pyrolytic products were identified by the NIST MS Library database. The peak area and retention time of each pyrolysis product were recorded and the main products were quantitatively analyzed by an external standard method [51].

2.5. Data analysis

The yield of produce monomer aromatics was calculated as follows:

$$Yield = \frac{m}{m_0} \times 100\% \quad (1)$$

where m is the mass of each product and m_0 is the PS weight before reaction, respectively.

The selectivity was calculated by the following equation:

$$Selectivity = \frac{m}{\sum m_i} \times 100\% \quad (2)$$

where $\sum m_i$ is the total mass of monomer aromatics (toluene, ethylbenzene, styrene, cumene, and α-methyl styrene).

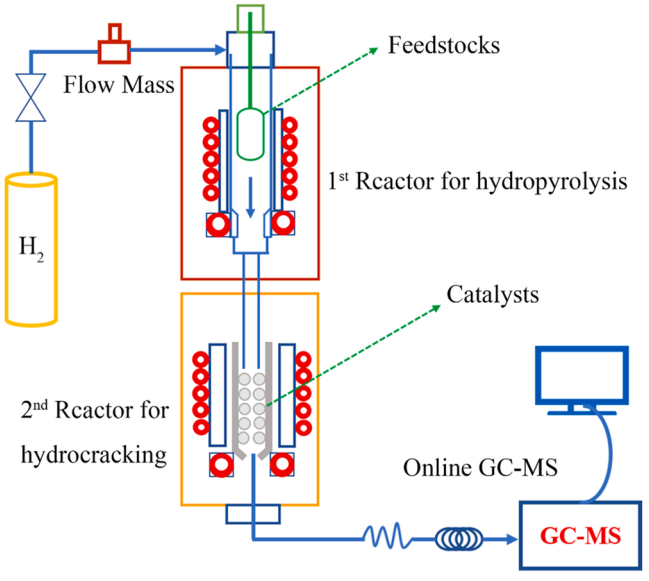

Fig. 1. Schematic diagram of the two-step pressurized flow-through fixed-bed reactor connected with an online GC/MS.

3. Results and discussion

3.1. Catalyst characterization

The XRD pattern of Fe_2N @ C is shown in Fig. 2. As shown in Fig. 2a, main diffraction peaks appear at 37.4°, 40.6°, 42.7°, 56.4°, 68.4° and 75.4° corresponding to the (0 2 1), (2 0 0), (1 2 1), (3 1 1) and (3 2 1) planes of Fe_2N (PDF#50–0958), respectively. It indicates the successful synthesis of iron nitride catalysts. The XRD spectrum of the Fe_2N @ C-H_2 catalyst after hydrogen reduction is shown in Fig. 2b, with two distinctive characteristic peaks at 44.7° and 65.0°, belonging to the (1 1 0) and (2 0 0) planes of Fe (PDF#06–0696), respectively, and no iron nitride phase was detected. The presence of Fe^0 provides active sites for hydrogenation, which is conducive to the adsorption and transfer of hydrogen.

The specific surface area and porosity of Fe_2N @ C were investigated using N_2 adsorption–desorption isotherms. The N_2 adsorption and desorption isotherms (Fig. 3a) is a type IV for Fe_2N @ C, with an H1 hysteresis loop, indicating that the presence of mesopores structure which facilitates the exposure of active centers and mass transfer [52]. The pore size distribution of the Fe_2N @ C catalyst is less than 10 nm, as shown in Fig. 3b. The relevant physical properties of the catalyst are summarized in Table S1. The BET surface area and total pore volume of Fe_2N @ C catalyst are 34 m^2/g and 0.043 cm^3/g, respectively.

The microstructure and particle distribution of the as-prepared Fe_2N @ C were studied by TEM and EDS mapping. Fig. 4a shows that uniform Fe_2O_3 nanocubes with ~200 nm size were synthesized through hydrothermal method. As exhibited in Fig. 4b, the Fe_2O_3 nanoparticles encapsulated by dopamine hydrochloride (Fig.S1) after annealing, dopamine hydrochloride is carbonized to form a porous carbon shell with a thickness of 35 nm, the Fe_2N @ C catalyst exhibits a typical core-shell structure, and no bare Fe_2N nanoparticles on the outer surface of the shell were observed. Fig. 4c shows a high-resolution transmission electron microscope, the fringe spacing of 0.34 nm matched well with the (1 1 0) lattice plane of Fe_2N. The EDS mapping (Fig. 4d-g) of the elements in the Fe_2N @ C composite shows the N, C, and Fe signals, observing the uniform distribution of Fe, N, and C without forming large iron particles.

The surface chemical composition and state of the as-prepared Fe_2N @ C are determined by XPS. As shown in Fig. 5a, the XPS spectrum of Fe_2N @ C confirmed the existence of Fe, N, C, and O elements. The high-resolution spectrum of Fe 2p is shown in Fig. 5b. As illustrated, the binding energies at 711.6 eV and 724.7 eV are attributed to the Fe^{3+} $2p_{3/2}$ and Fe^{3+} $2p_{1/2}$, the binding energies of Fe^{2+} $2p_{3/2}$ and Fe^{2+} $2p_{1/2}$ are 709.7 and 722.7 eV, reflecting the co-existence of FeO and Fe_2O_3 in Fe_2N @ C. Furthermore, the peaks situated at 708.2 eV and 719.5 eV correspond to Fe-N and Fe^{3+} satellite, respectively [50]. The high-resolution XPS of the N 1 s peak spectrum (Fig. 5c) can be deconvoluted into four peaks, including Fe-N (396.9 eV), pyridinic-N (398.3 eV), pyrrolic-N (399.8 eV), and graphitic-N (400.9 eV) [52]. In general, Pyridinic-N and pyrrolic -N have lone pair electrons that can be used as metal-coordination sites and play a dominant role in anchoring the active sites and enhancing their dispersion [53–55]. Therefore, Fe directly bonded with pyridinic-N or pyrrolic-N in Fe_2N @ C [56]. The XPS spectrum of Fe_2N @ C-H_2 after H_2 reduction is shown in Fig. 5d. The high-resolution spectrum of Fe 2p is shown in Fig. 5e. In contrast to the Fe 2p high-resolution spectrum of Fe_2N @ C, the presence of metallic iron was observed at the binding energy of 706.5 eV in the Fe 2p high-resolution spectrum of Fe_2N @ C-H_2 [57]. On the one hand, the presence of metallic Fe phase provides active sites for hydrogen activation and promotes H-H breakage. On the other hand, it provides electrons to C and N, which are endowed with adsorption and activation sites for hydrogen. Fig. 5f shows the high-resolution spectrum of N 1 s after hydrogen reduction of Fe_2N @ C. As illustrated, the N 1 s spectra were deconvoluted into three peaks (pyridinic N, pyrrolic N, and quaternary N), the presence of Fe-N species was not found. The XPS

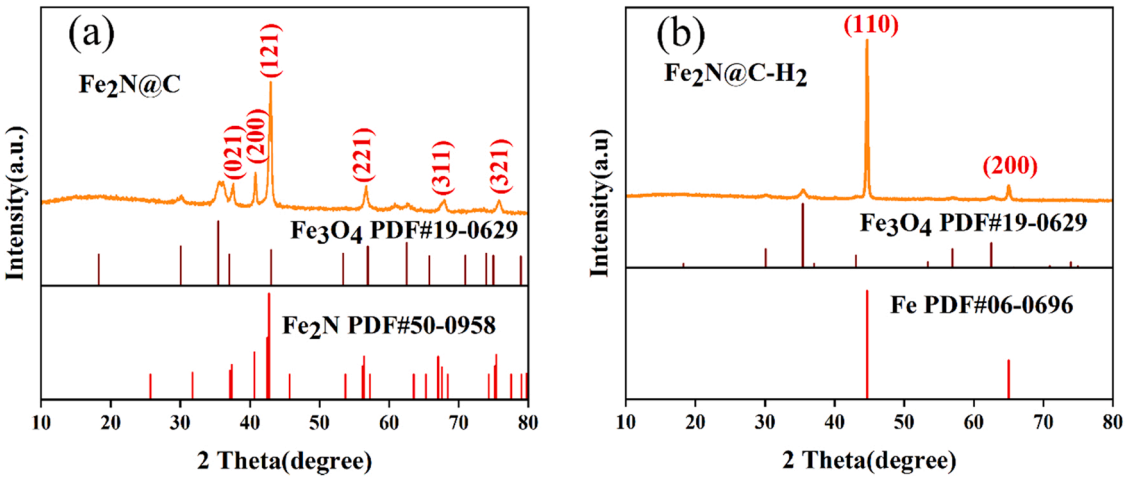

Fig. 2. XRD pattern of (a) Fe_2N @ C; (b) Fe_2N @ C after H_2 reduction.

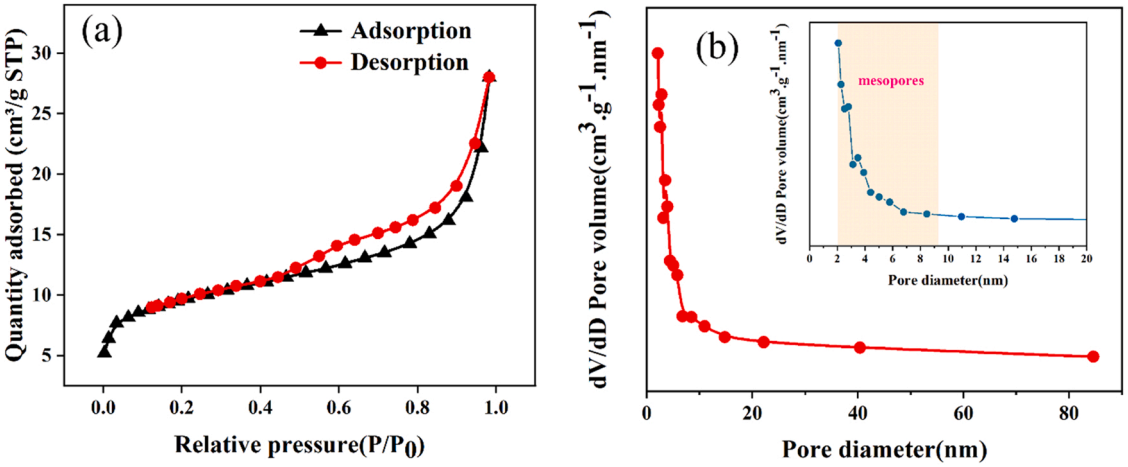

Fig. 3. Nitrogen adsorption-desorption isotherms (a) and pore size distribution (b) of Fe_2N @ C catalyst.

spectrums of Fe_2N @ C and Fe_2N @ C-H_2 are agreed well with the results obtained from XRD (Fig. 2b).

The strength and density of acid sites of Fe_2N @ C catalyst were characterized by NH_3-TPD, and the results are shown in Fig. 6a. Two obvious ammonia desorption peaks appear at 380 ℃ (low temperature region) and 550 ℃ (high temperature region), corresponding to weak acid sites (0.116 mmol/g, Table S2) and strong acid sites (1.225 mmol/g, Table S2), respectively. The presence of acidic sites in the Fe_2N @ C catalyst facilitates the cleavage of C-C bonds in PS plastics [58]. The thermal stability of the Fe_2N @ C catalyst was analyzed by TGA. Fig. 6b exhibits the TGA curve of the Fe_2N @ C. The volatilization of water or gas molecules adsorbed on the catalyst surface at temperatures below 100 °C, with a mass loss rate of 1.4%; and a major thermal decomposition occurs between 400 °C and 600 °C, with a weight loss of 23.1%. Raman spectrums were used to investigate carbon structure of Fe_2N @ C. Raman spectrums are shown in Fig. 6c, two distinctive peaks are located at 1360 cm^{-1} (D band) and 1570 cm^{-1} (G band). In general, the G band is related to the sp^2-hybridization of graphitic carbon, and D band is associated with amorphous or disordered carbon. I_D/I_G is used to characterize the degree of graphitization. As illustrated, the I_D/I_G value of Fe_2N @ C is 1.04, indicating the presence of more disordered carbons, which are beneficial to the formation of active centers [59].

3.2. Optimization of reaction process

Appropriate operating conditions are of particular importance for the efficient utilization of PS plastics. Thermal degradation properties of polystyrene were investigated by TGA. Fig. S2 shows the thermogravimetric curve of polystyrene. The thermal degradation of polystyrene starts at 340 °C and reaches a maximum degradation of 99.8% at 480 °C. Therefore, to fully degrade PS plastic, the hydropyrolysis temperature of polystyrene was set at 480 °C. Moreover, hydrocracking temperature (280 ℃) and reaction pressure (0.2 MPa) are controlled under relatively mild conditions.

It is well known that catalyst loading is one of the important parameters that has a significant impact on the quality of liquid products obtained from plastic deconstruction. Specifically, catalyst loading affects the surface contact degree between pyrolysis vapors and catalysts [60]. The impact of different catalyst loadings on the yield of ethylbenzene was explored. The experimental results are shown in Fig. 7a. As expected, the obtained ethylbenzene yield was increased from 39 to 81 wt% as the catalyst loading was increased from 1.2 to 5 mg. Correspondingly, the monomer styrene yield was decreased (from 38.5 to 0.0 wt%) with increasing the catalyst loading (Total ion chromatogram (TIC) shown in Fig. S3). Additionally, increasing catalyst loading from 1.2 to 5 mg resulted in an increase in ethylbenzene selectivity from 45.3% to 91.3% (Fig. 7b). Notably, a further increase in catalyst loading (from 5 to 10 mg) did not significantly improve ethylbenzene yield and

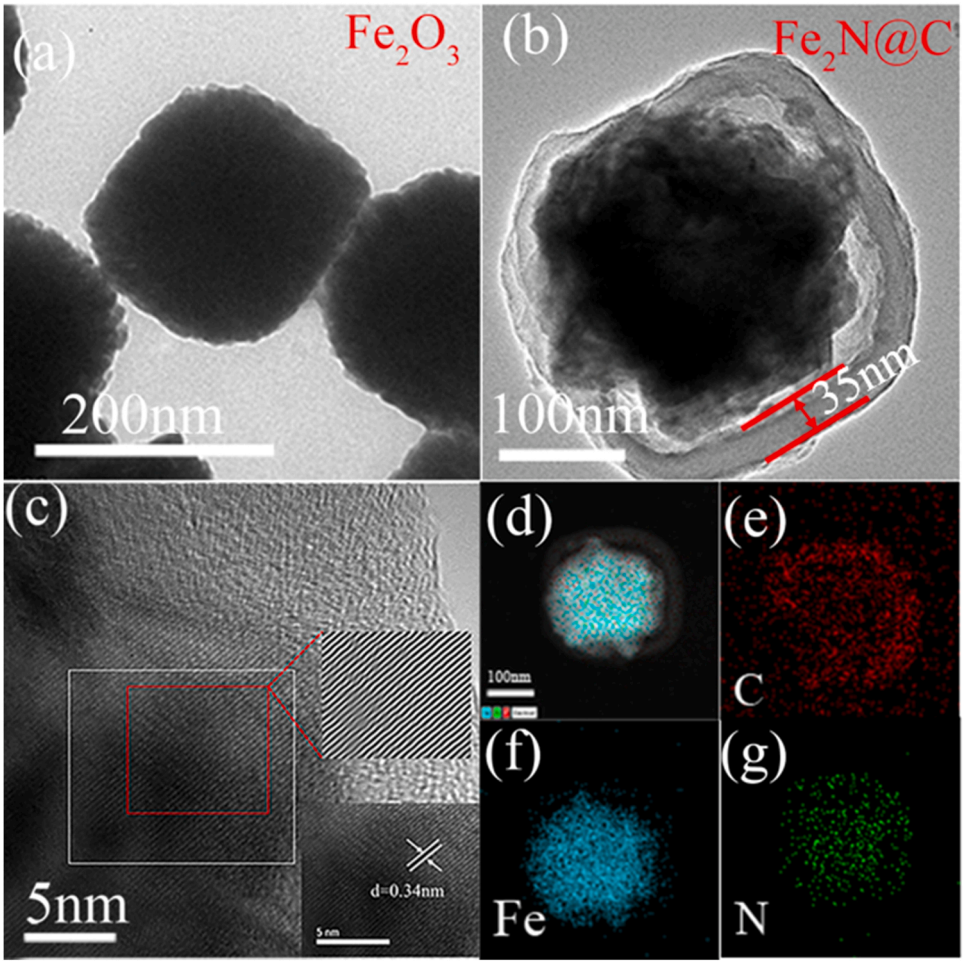

Fig. 4. (a) TEM images of Fe_2O_3; (b) TEM images of Fe_2N @ C; (c) HRTEM images of Fe_2N @ C; (d-g) TEM-EDS elemental mapping images of Fe_2N @ C.

its selectivity. Thus, the optimum catalyst loading for improving the ethylbenzene yield is 5 mg. Mainly because the high catalyst loading results in sufficient surface contact between Fe_2N @ C and the styrene intermediate, where styrene is hydrogenated to ethylbenzene. Therefore, the contact degree could be improved by elevating the catalyst loadings to further increase the yield of target products. For instance, Aljabri et al. [61] investigated the effect of catalyst loadings on the catalytic conversion of polystyrene, and the results showed that the obtained liquid yield was increased from 71% to 91% as the catalyst loading was increased from 100 to 400 mg.

Overall, to maximize the yield of ethylbenzene, the optimal hydropyrolysis temperature, hydrocracking temperature, reaction pressure, and the mass ratio of catalyst to PS could be maintained at 480 ℃, 280 ℃, 0.2 MPa, 5:0.3, respectively.

3.3. Catalytic activity evaluation

The hydropyrolysis of polystyrene and the subsequent gas-phase hydrocracking of the resulting primary intermediates were investigated in a two-step pressurized fixed-bed reactor. The effect of catalysts on the thermal degradation of PS plastic by employing commercial metal nitrides as catalysts were preliminarily investigated. The chromatograms obtained from catalytic conversion of PS over different commercial metal nitrides are illustrated in Fig. 8a. As expected, the pyrolysis of polystyrene without catalysts generated 83.5 wt% monomers containing 65.7 wt% styrene, 11.5 wt% ethylbenzene, 1.02 wt% toluene, 0.6 wt% cumene, and 4.7 wt% α-methyl styrene, respectively (Fig. 8b). Generally, unsaturated styrene in pyrolysis products limits the application of upcycling PS plastics into drop-in liquid fuels. From the viewpoint of producing liquid fuels, these styrene and α-methyl styrene needs to be hydrocracked. Metal nitrides are widely used in hydrogenation because of their good ability to adsorb and dissociate hydrogen [48,62]. For instance, Zhao et al. [46] synthesized an iron nitride catalyst for hydrogenation of CO_2 to C_{2+} hydrocarbons, iron nitride exhibits outstanding performance toward CO_2 hydrogenation to C_{2+} hydrocarbons (C_{2+} selectivity: 53.96%; C_2-C_4 selectivity: 31.03%).

To verify the hydrogenation activity of metal nitrides, we investigated the tandem hydropyrolysis/hydrocracking of PS over five commercial metal nitride catalysts (TaN, Cr_2N, NNb, GdN, and FeN, TIC chromatographs shown in Fig. S4). The catalyst loading was controlled at 50 mg for each experiment (because of the high density of metal nitride catalysts) to provide sufficient contact between styrene-based intermediates and catalysts. As shown in Fig. S5, toluene, ethylbenzene, styrene, and α-methyl styrene products were observed over the five commercial metal nitrides. However, commercial TaN, Cr_2N, NNb, and GdN catalysts illustrated very low activity in producing ethylbenzene, generating negligible ethylbenzene with the yield of 4.6, 4.4, 3.9, and 5.5 wt%, respectively. In contrast, the product distribution is dominated by styrene with the yield of 73.1 wt%, 72.5 wt%, 74.7 wt%, and 72 wt%, respectively. The use of commercial TaN, Cr_2N, NNb, and GdN catalysts did not promote the formation of ethylbenzene, this probably attributed to the absence of styrene hydrocracking active sites. Interestingly, when the conversion of polystyrene was conducted over commercial FeN catalyst, these styrene-based intermediates can be further hydrocracked, leading to an increase in ethylbenzene yield to 68.1 wt% (Fig. S6). Among all commercial metal nitride catalysts (TaN,

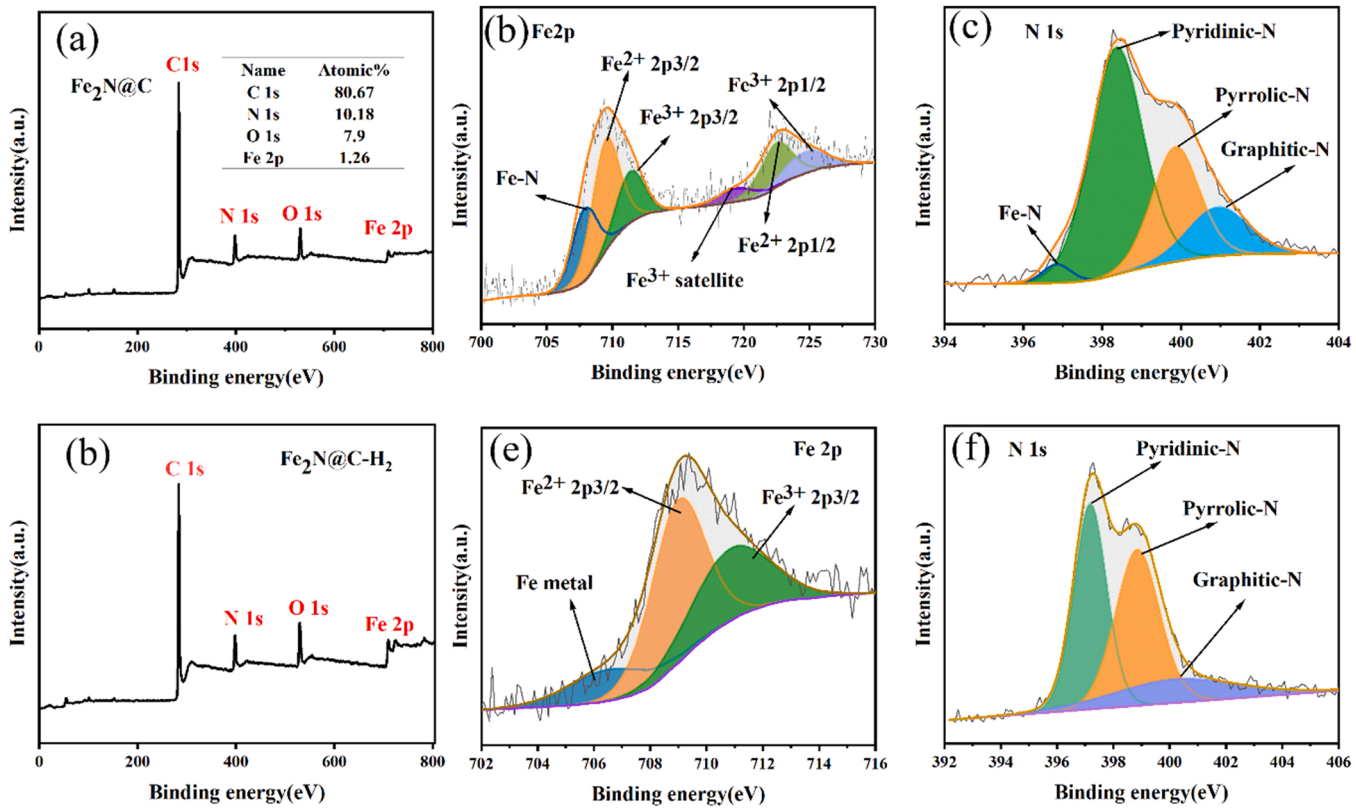

Fig. 5. XPS spectra of Fe_2N @ C (a) survey spectra; (b) Fe 2p spectra; (c) N 1 s spectra and XPS spectra of Fe_2N @ C-H_2 (d) survey spectra; (e) Fe 2p spectra; (f) N 1 s spectra.

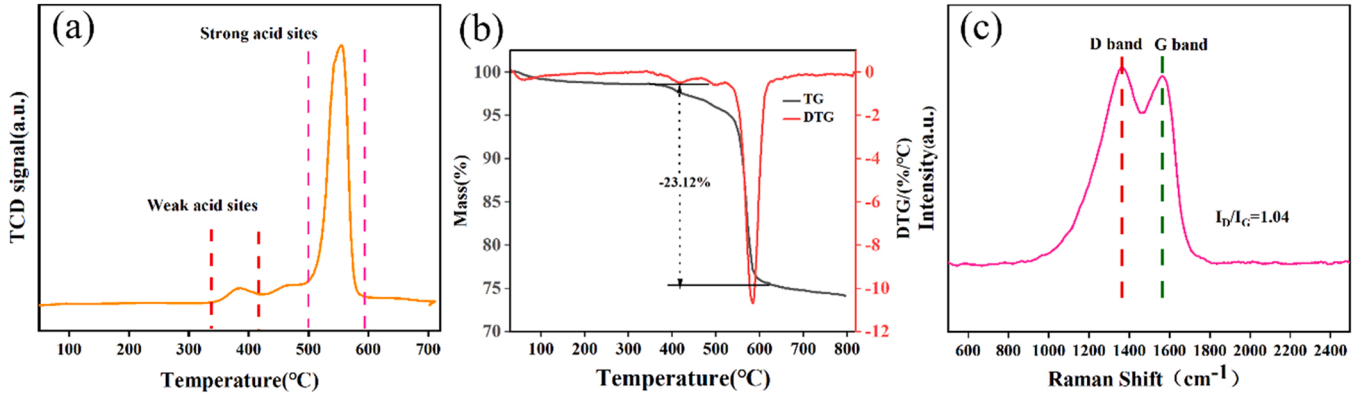

Fig. 6. (a) NH_3-TPD of Fe_2N @ C; (b) Thermogravimetric curve of Fe_2N @ C; (c) Raman spectroscopy of Fe_2N @ C.

Cr_2N, NNb, GdN, and FeN), only Fe-based nitrides exhibit considerable activity in generating ethylbenzene from styrene intermediate under a high catalyst loading of 50 mg.

To further improve the yield of ethylbenzene, Fe_2N, and Fe_2N @ C catalysts were synthesized. Fig. 8b shows the yield of liquid oil as a function of catalyst type. When synthetic Fe_2N was used as a catalyst, the yield of ethylbenzene increased to 63.3 wt%. Correspondingly, the yield of styrene decreased to 12.9 wt%. As expected, the use of as-prepared Fe_2N dramatically promoted the formation of ethylbenzene as a ~12.9-fold increase was reached compared to that over commercial FeN (catalyst loading of 5 mg). Noteworthy, Fe_2N @ C gave an exceptional yield of ethylbenzene and a high ethylbenzene selectivity. Specifically, the yield of ethylbenzene obtained from Fe_2N @ C catalysis was 81 wt%, which is much higher than that observed over pure Fe_2N and commercial FeN (63.3 wt% and 4.9 wt%, respectively, TIC chromatographs shown in Fig. 8a). In addition, the ethylbenzene selectivity obtained from Fe_2N @ C catalysis was 91.3%, which was 16.6% higher than that derived from Fe_2N. The carbon doping drastically boosted the catalytic performance of Fe_2N. For example, Wang et al. [63] reported the Co^0-Co_3O_4/N-doped carbon nanotubes as hydrogenation catalysts for nitroarenes, the catalyst exhibits good catalytic activity and excellent selectivity (>99%) for substituted nitroarenes under relatively mild conditions. Density functional calculations show that inner Co^0 and N species on the carbon shell can decrease the dissociation energies of H_2, enabling the carbon shell to activate hydrogen. The introduction of inert porous carbon shells as a protective layer can effectively delay the deactivation of catalyst without hindering the accessibility of primary intermediates, prevent the aggregation of catalysts, and enhance the activity and stability of catalyst through interfacial electron effect [46].

To understand the hydrogenation activity of Fe_2N @ C, we further

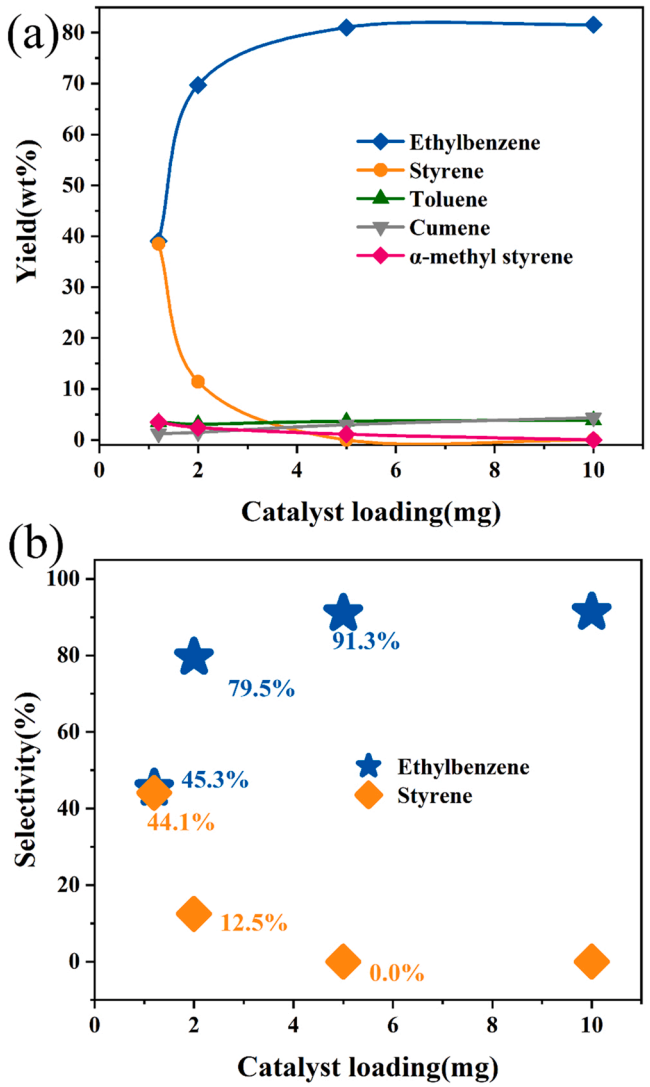

Fig. 7. (a) Product distribution as a function of Fe_2N @ C catalyst loading; (b) Product selectivity as a function of Fe_2N @ C catalyst loading. Reaction conditions: hydropyrolysis temperature 480 ℃, hydrocracking temperature: 280 ℃, PS weight: 0.3 ± 0.05 mg, and H_2 pressure 0.2 MPa.

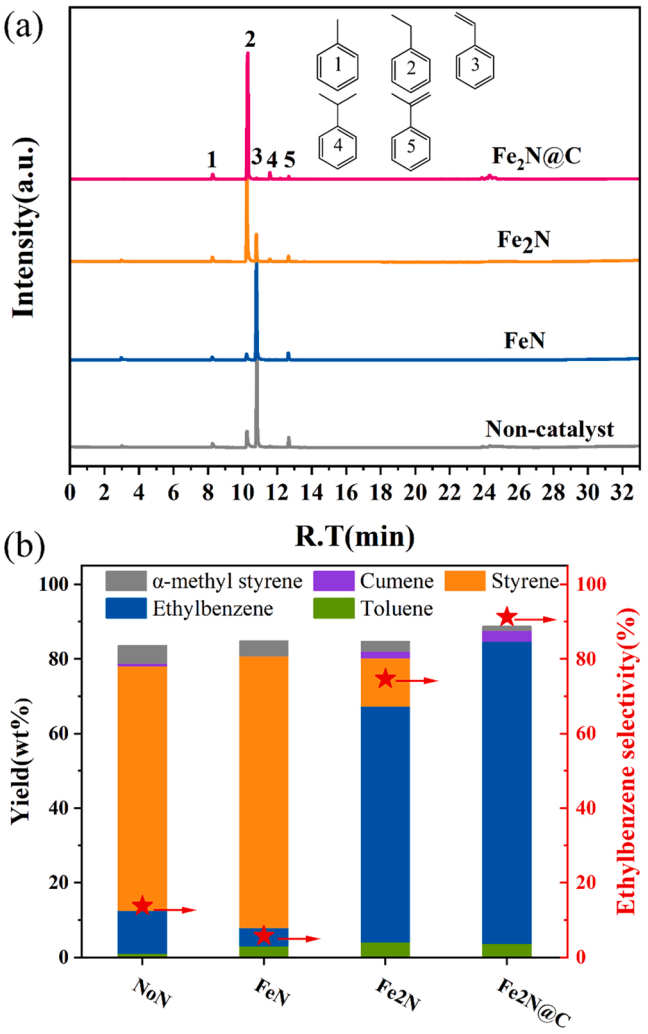

Fig. 8. (a) TIC chromatogram of different types of iron nitride catalyzed PS plastics. (b) Major product distribution of polystyrene under different types of iron nitride catalyzed conversions. Reaction conditions: catalyst to feedstock ratio 5:0.3; hydropyrolysis temperature 480 ℃, hydrocracking temperature 280 ℃; H_2 pressure 0.2 MPa.

explored the catalytic conversion of styrene model compound over metal nitrides, and the results are shown in Fig. S7. As expected, Fe-based nitrides exhibit good hydrogenation activity, and the maximum conversion of 100% was observed over a Fe_2N @ C catalyst. When the catalytic hydrogenation of styrene was conducted over FeN catalyst, a 70% styrene conversion was observed with ethylbenzene being the only product. However, the use of NC catalyst did not promote the conversion of styrene to ethylbenzene. Obviously, the introduction of metallic Fe phase greatly promoted the catalytic conversion of styrene. Based on the above experiments, we suggest that the good catalytic hydrogenation activity of Fe_2N @ C was attributed to the synergistic effect between iron nitride and N-doped carbon layers because the catalyst shows better catalytic performance than NC and FeN. Specifically, pyridinic-N and pyrrolic-N provide coordination sites to metallic Fe phase to form the active Fe-N sites (Fig. 5) [44]. Furthermore, N embedded in the carbon shell matrix can cause the charge delocalization, and tune the carbon shell from inert to active [48]. Moreover, the mesoporous structure (Fig. 3) of Fe_2N @ C offers additional advantages in facilitating the mass transfer of reactants and providing more active centers. For example, Liu et al.[64] reported a N-doped carbon layer encapsulated Fe_2N as an efficient catalyst for oxygen reduction reaction. The results showed that high activity could be due to the synergistic effect of Fe_2N with the N-doped graphitic carbon layers and the mesoporous structure facilitating the mass transfer.

In general, pyrolysis of polystyrene consists of two main reaction pathways, including gradual degradation to produce monomers (styrene, ethylbenzene, toluene, cumene, and α-methyl styrene) and volatile oligomers (dimers) [65]. The catalytic hydrocracking of styrene and α-methyl styrene takes place in the Fe_2N @ C catalyst active centers. Scheme 1 proposes a possible reaction pathway for the catalytic hydrocracking of polystyrene to ethylbenzene. The presence of metallic iron phase in the Fe_2N @ C catalyst after H_2 reduction provides the active site for H_2 activation and promotes H-H cleavage. Moreover, due to interface electron effects, the iron endows electrons to C and N, making NC from inert to active and able to adsorb hydrogen molecules [48,66]. Specifically, it mainly includes three aspects: (i) Hydrogen diffuse onto the surface of Fe_2N @ C is activated by Fe^0; meanwhile Fe provides electrons to NC; (ii) dissociative adsorption of the hydrogen molecule bonded to the NC; (iii) the adsorbed hydrogen participates in the hydrogenation reaction. Besides, due to the presence of acidic sites, volatile oligomers activated by acid sites decompose to styrene, ethylbenzene, toluene, and cumene [58]. In summary, the excellent hydrogenation activity of Fe_2N @ C is attributed to the efficient synergy of

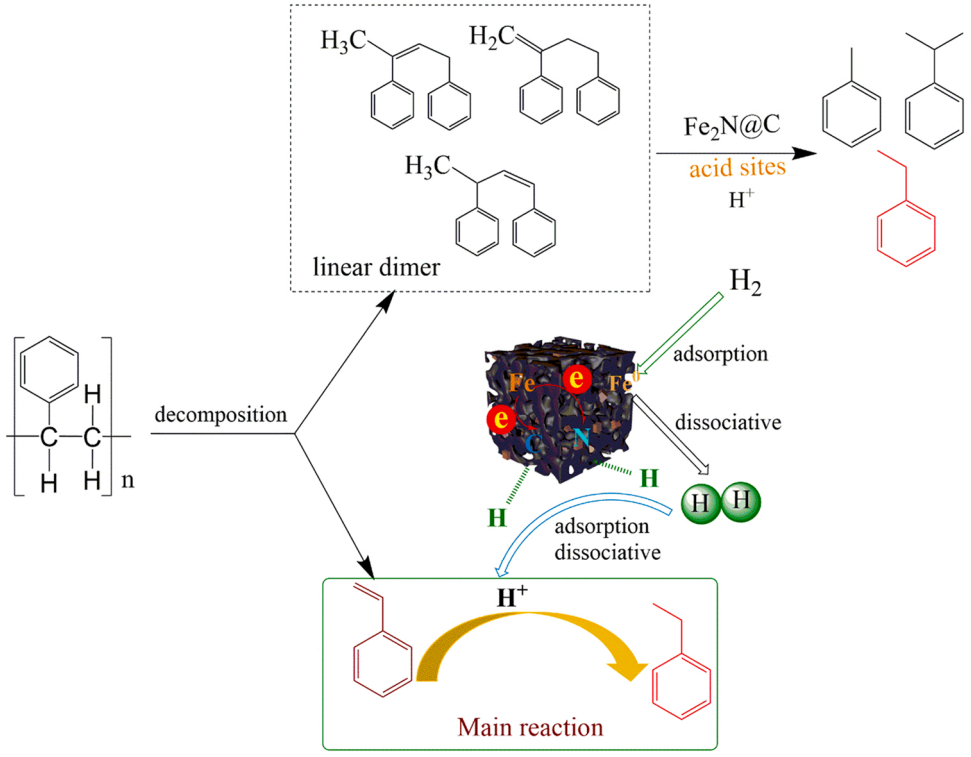

Scheme 1. Proposed reaction pathway for catalytic conversion of polystyrene to generate ethylbenzene.

acid site-mediated C-C bond activation and metal-based selective hydrogenation.

4. Conclusion

We demonstrated that the Fe_2N @ C exhibited high activity in converting PS wastes into ethylbenzene under relatively mild conditions. XRD and XPS results revealed that the presence of metallic Fe phase provides active sites for hydrogenation, and the formation of pyridinic-N and pyrrolic -N plays a key role in anchoring the active sites. Furthermore, Fe_2N @ C catalyst exhibits a high content of acid sites, which is conducive to the cleavage of C-C bonds, as shown by the NH_3-TPD. N_2 adsorption-desorption indicates that the presence of mesopores properties, which facilitates the mass transfer and expose more active sites. The ethylbenzene obtained from the Fe_2N @ C catalysis was ~16 times higher than that of the commercial iron nitride (FeN) under hydropyrolysis temperature of 480 ℃, hydrocracking temperature of 280 ℃, and low H_2 pressure of 0.2 MPa. Meanwhile, the ethylbenzene selectivity obtained from Fe_2N @ C was 91.3%, which was 16.6% higher than that derived from Fe_2N.

CRediT authorship contribution statement

Zhukun Zhang: Conceptualization, Methodology, Investigation, Writing – original draft. **Dongxian Li:** Conceptualization, Methodology, Resources. **Jia Wang:** Conceptualization, Methodology, Investigation, Funding acquisition, Writing – review & editing. **Jianchun Jiang:** Supervision, Project administration, Funding acquisition, Writing – review & editing.

Declaration of Competing Interest

The authors declare that they have no known competing financial interests or personal relationships that could have appeared to influence the work reported in this paper.

Data Availability

The authors do not have permission to share data.

Acknowledgments

The authors are grateful to the Natural Science Foundation of Jiangsu Province (No. BK2020789), National Natural Science Foundation of China (No. 52006106), Jiangsu Province Key Laboratory of Biomass Energy and Materials (JSBEM-S-202002), and China Postdoctoral Science Foundation (No. 2020TQ0154).

Appendix A. Supporting information

Supplementary data associated with this article can be found in the online version at doi:10.1016/j.apcatb.2022.122164.

References

[1] G. Lopez, M. Artetxe, M. Amutio, J. Alvarez, J. Bilbao, M. Olazar, , Recent advances in the gasification of waste plastics. A critical overview, Renew. Sust. Energ. Rev. 82 (2018) 576–596.
[2] M.S. Qureshi, A. Oasmaa, H. Pihkola, I. Deviatkin, A. Tenhunen, J. Mannila, H. Minkkinen, M. Pohjakallio, J. Laine-Ylijoki, Pyrolysis of plastic waste: Opportunities and challenges, J. Anal. Appl. Pyrolysis 152 (2020).
[3] S.D. Anuar Sharuddin, F. Abnisa, W.M.A. Wan Daud, M.K. Aroua, A review on pyrolysis of plastic wastes, Energ. Convers. Manag. 115 (2016) 308–326.
[4] G. Faraca, T. Astrup, Plastic waste from recycling centres: characterisation and evaluation of plastic recyclability, Waste Manag. 95 (2019) 388–398.
[5] A. Rahimi, J.M. García, Chemical recycling of waste plastics for new materials production, Nat. Rev. Chem. 1 (2017).
[6] Z. Wang, K.G. Burra, T. Lei, A.K. Gupta, Co-pyrolysis of waste plastic and solid biomass for synergistic production of biofuels and chemicals-a review, Prog. Energ. Combust. 84 (2021).
[7] C. Wang, H. Han, Y. Wu, D. Astruc, Nanocatalyzed upcycling of the plastic wastes for a circular economy, Coord. Chem. Rev. 458 (2022).
[8] K.V.S. Rajmohan, C. Ramya, M. Raja Viswanathan, S. Varjani, Plastic pollutants: effective waste management for pollution control and abatement, Curr. Opin. Environ. Sci. Health 12 (2019) 72–84.
[9] N. Ahmad, N. Ahmad, I.M. Maafa, U. Ahmed, P. Akhter, N. Shehzad, U.-e-s Amjad, M. Hussain, M. Javaid, Conversion of poly-isoprene based rubber to value-added

chemicals and liquid fuel via ethanolysis: Effect of operating parameters on product quality and quantity, Energy 191 (2020).
[10] N. Ahmad, N. Ahmad, I.M. Maafa, U. Ahmed, P. Akhter, N. Shehzad, U.-e-s Amjad, M. Hussain, Thermal conversion of polystyrene plastic waste to liquid fuel via ethanolysis, Fuel 279 (2020).
[11] T. Lee, S. Jung, Y.K. Park, T. Kim, H. Wang, D.H. Moon, E.E. Kwon, Catalytic pyrolysis of polystyrene over steel slag under CO_2 environment, J. Hazard. Mater. 395 (2020), 122576.
[12] T. Kan, V. Strezov, T.J. Evans, Lignocellulosic biomass pyrolysis: a review of product properties and effects of pyrolysis parameters, Renew. Sust. Energ. Rev. 57 (2016) 1126–1140.
[13] S. Wang, G. Dai, H. Yang, Z. Luo, Lignocellulosic biomass pyrolysis mechanism: a state-of-the-art review, Prog. Energ. Combust. 62 (2017) 33–86.
[14] S. Oh, J. Lee, S.S. Lam, E.E. Kwon, J.M. Ha, D.C.W. Tsang, Y.S. Ok, W.H. Chen, Y. K. Park, Fast hydropyrolysis of biomass conversion: a comparative review, Bioresour. Technol. 342 (2021), 126067.
[15] T. Maqsood, J. Dai, Y. Zhang, M. Guang, B. Li, Pyrolysis of plastic species: a review of resources and products, J. Anal. Appl. Pyrolysis 159 (2021).
[16] Y. Liu, J. Qian, J. Wang, Pyrolysis of polystyrene waste in a fluidized-bed reactor to obtain styrene monomer and gasoline fraction, Fuel Process. Technol. 63 (2000) 45–55.
[17] R.S. Chauhan, S. Gopinath, P. Razdan, C. Delattre, G.S. Nirmala, R. Natarajan, Thermal decomposition of expanded polystyrene in a pebble bed reactor to get higher liquid fraction yield at low temperatures, Waste Manag. 28 (2008) 2140–2145.
[18] Z. Huang, M. Shanmugam, Z. Liu, A. Brookfield, E.L. Bennett, R. Guan, D.E. Vega Herrera, J.A. Lopez-Sanchez, A.G. Slater, E.J.L. McInnes, X. Qi, J. Xiao, Chemical recycling of polystyrene to valuable chemicals via selective acid-catalyzed aerobic oxidation under visible light, J. Am. Chem. Soc. 144 (2022) 6532–6542.
[19] J.A. Onwudili, N. Insura, P.T. Williams, Composition of products from the pyrolysis of polyethylene and polystyrene in a closed batch reactor: effects of temperature and residence time, J. Anal. Appl. Pyrolysis 86 (2009) 293–303.
[20] Ue.S. Amjad, M. Ishaq, Hu Rehman, N. Ahmad, L. Sherin, M. Hussain, M. Mustafa, Diesel and gasoline like fuel production with minimum styrene content from catalytic pyrolysis of polystyrene, Environ. Prog. Sustain. 40 (2020).
[21] E.G. Fuentes-Ordóñez, J.A. Salbidegoitia, J.L. Ayastuy, M.A. Gutiérrez-Ortiz, M. P. González-Marcos, J.R. González-Velasco, High external surface Pt/zeolite catalysts for improving polystyrene hydrocracking, Catal. Today 227 (2014) 163–170.
[22] E.G. Fuentes-Ordóñez, J.A. Salbidegoitia, M.P. González-Marcos, J.L. Ayastuy, M. A. Gutiérrez-Ortiz, J.R. González-Velasco, Pt/ITQ-6 zeolite as a bifunctional catalyst for hydrocracking of waste plastics containing polystyrene, J. Mater. Cycles Waste 17 (2014) 465–475.
[23] M. Utami, K. Wijaya, W. Trisunaryanti, Pt-promoted sulfated zirconia as catalyst for hydrocracking of LDPE plastic waste into liquid fuels, Mater. Chem. Phys. 213 (2018) 548–555.
[24] M.P. González-Marcos, E.G. Fuentes-Ordóñez, J.A. Salbidegoitia, J.R. González-Velasco, Optimization of supports in bifunctional supported Pt catalysts for polystyrene hydrocracking to liquid fuels, Top. Catal. 64 (2020) 224–242.
[25] J. Weitkamp, Catalytic hydrocracking—mechanisms and versatility of the process, ChemCatChem 4 (2012) 292–306.
[26] D. Munir, M.R. Usman, Catalytic hydropyrolysis of a model municipal waste plastic mixture over composite USY/SBA-16 catalysts, J. Anal. Appl. Pyrolysis 135 (2018) 44–53.
[27] D. Munir, M.F. Irfan, M.R. Usman, Hydrocracking of virgin and waste plastics: a detailed review, Renew. Sust. Energ. Rev. 90 (2018) 490–515.
[28] Y. Jing, Y. Wang, S. Furukawa, J. Xia, C. Sun, M.J. Hulsey, H. Wang, Y. Guo, X. Liu, N. Yan, Towards the circular economy: converting aromatic plastic waste back to Arenes over a Ru/Nb_2O_5 catalyst, Angew. Chem. Int. Ed. 60 (2021) 5527–5535.
[29] L. Yao, J. King, D. Wu, J. Ma, J. Li, R. Xie, S.S.C. Chuang, T. Miyoshi, Z. Peng, Non-thermal plasma-assisted rapid hydrogenolysis of polystyrene to high yield ethylene, Nat. Commun. 13 (2022) 885.
[30] J. Wang, J. Jiang, X. Wang, S. Liu, X. Shen, X. Cao, Y. Sun, L. Dong, X. Meng, A. J. Ragauskas, Y. Wang, Polyethylene upcycling to fuels: narrowing the carbon number distribution in n-alkanes by tandem hydropyrolysis/hydrocracking, Chem. Eng. J. 444 (2022).
[31] J.E. Rorrer, G.T. Beckham, Y. Roman-Leshkov, Conversion of polyolefin waste to liquid alkanes with ru-based catalysts under mild conditions, JACS Au 1 (2021) 8–12.
[32] K.L. Sanchez-Rivera, G.W. Huber, Catalytic hydrogenolysis of polyolefins into alkanes, ACS Cent. Sci. 7 (2021) 17–19.
[33] D.P. Serrano, J.M. Escola, L. Briones, M. Arroyo, Hydroprocessing of the LDPE thermal cracking oil into transportation fuels over Pd supported on hierarchical ZSM-5 catalyst, Fuel 206 (2017) 190–198.
[34] J.M. Escola, D.P. Serrano, J. Aguado, L. Briones, Hydroreforming of the LDPE thermal cracking oil over hierarchical Ni/Beta catalysts with different Ni particle size distributions, Ind. Eng. Chem. Res. 54 (2015) 6660–6668.
[35] D.P. Serrano, J.M. Escola, L. Briones, S. Medina, A. Martínez, Hydroreforming of the oils from LDPE thermal cracking over Ni–Ru and Ru supported over hierarchical Beta zeolite, Fuel 144 (2015) 287–294.
[36] E.G. Fuentes-Ordóñez, J.A. Salbidegoitia, M.P. González-Marcos, J.R. González-Velasco, Mechanism and kinetics in catalytic hydrocracking of polystyrene in solution, Polym. Degrad. Stab. 124 (2016) 51–59.
[37] U.E. Amjad, A. Tajjamal, A. Ul-Hamid, A. Faisal, S.A.H. Zaidi, L. Sherin, A. Mir, M. Mustafa, N. Ahmad, M. Hussain, Y.K. Park, Catalytic cracking of polystyrene pyrolysis oil: Effect of Nb_2O_5 and NiO/Nb_2O_5 catalyst on the liquid product composition, Waste Manag. 141 (2022) 240–250.
[38] S. Jin, K. Cui, H. Guan, M. Yang, L. Liu, C. Lan, Preparation of mesoporous MCM-41 from natural sepiolite and its catalytic activity of cracking waste polystyrene plastics, Appl. Clay Sci. 56 (2012) 1–6.
[39] M. Nagai, Transition-metal nitrides for hydrotreating catalyst—synthesis, surface properties, and reactivities, Appl. Catal. A: Gen. 322 (2007) 178–190.
[40] V.R.B. Gurram, S.S. Enumula, R.R. Chada, K.S. Koppadi, D.R. Burri, S.R. R. Kamaraju, Synthesis and industrial catalytic applications of binary and ternary molybdenum nitrides: a review, Catal. Surv. Asia 22 (2018) 166–180.
[41] E. Furimsky, Metal carbides and nitrides as potential catalysts for hydroprocessing, Appl. Catal. A Gen. 240 (2003) 1–28.
[42] Z. Lin, S.R. Denny, J.G. Chen, Transition metal carbides and nitrides as catalysts for thermochemical reactions, J. Catal. 404 (2021) 929–942.
[43] X. Liu, H. Liu, C. Chen, L. Zou, Y. Li, Q. Zhang, B. Yang, Z. Zou, H. Yang, Fe_2N nanoparticles boosting FeNx moieties for highly efficient oxygen reduction reaction in Fe-N-C porous catalyst, Nano Res. 12 (2019) 1651–1657.
[44] J. Han, H. Bao, J.-Q. Wang, L. Zheng, S. Sun, Z.L. Wang, C. Sun, 3D N-doped ordered mesoporous carbon supported single-atom Fe-N-C catalysts with superior performance for oxygen reduction reaction and zinc-air battery, Appl. Catal. B: Environ. 280 (2021).
[45] J. Liu, C. Wang, H. Sun, H. Wang, F. Rong, L. He, Y. Lou, S. Zhang, Z. Zhang, M. Du, CoOx/CoNy nanoparticles encapsulated carbon-nitride nanosheets as an efficiently trifunctional electrocatalyst for overall water splitting and Zn-air battery, Appl. Catal. B: Environ. 279 (2020).
[46] B. Zhao, M. Sun, F. Chen, Y. Shi, Y. Yu, X. Li, B. Zhang, Unveiling the activity origin of iron nitride as catalytic material for efficient hydrogenation of CO_2 to C_{2+} hydrocarbons, Angew. Chem. Int. Ed. 60 (2021) 4496–4500.
[47] R. Ding, J. Zhang, J. Zhang, Z. Li, C. Wang, M. Chen, Core-shell Fe_2N@amorphous carbon nanocomposite-filled 3D graphene framework: an additive-free anode material for lithium-ion batteries, Chem. Eng. J. 360 (2019) 1063–1070.
[48] J. Song, Z.-F. Huang, L. Pan, K. Li, X. Zhang, L. Wang, J.-J. Zou, Review on selective hydrogenation of nitroarene by catalytic, photocatalytic and electrocatalytic reactions, Appl. Catal. B: Environ. 227 (2018) 386–408.
[49] X.Y. Yu, H. Hu, Y. Wang, H. Chen, X.W. Lou, Ultrathin MoS(2) nanosheets supported on n-doped carbon nanoboxes with enhanced lithium storage and electrocatalytic properties, Angew. Chem. Int. Ed. (2015) 7395–7398.
[50] X. Cui, X. Liang, J. Chen, W. Gu, G. Ji, Y. Du, Customized unique core-shell Fe_2N@ N-doped carbon with tunable void space for microwave response, Carbon 156 (2020) 49–57.
[51] Q. Lu, M.-x Zhou, W.-t Li, X. Wang, M.-s Cui, Y.-p Yang, Catalytic fast pyrolysis of biomass with noble metal-like catalysts to produce high-grade bio-oil: Analytical Py-GC/MS study, Catal. Today 302 (2018) 169–179.
[52] X. Huang, Z. Yang, B. Dong, Y. Wang, T. Tang, Y. Hou, In situ Fe_2N@N-doped porous carbon hybrids as superior catalysts for oxygen reduction reaction, Nanoscale 9 (2017) 8102–8106.
[53] F. Wang, J. Jiang, K. Wang, Q. Zhai, F. Long, P. Liu, J. Feng, H. Xia, J. Ye, J. Li, J. Xu, Hydrotreatment of lipid model for diesel-like alkane using nitrogen-doped mesoporous carbon-supported molybdenum carbide, Appl. Catal. B: Environ. 242 (2019) 150–160.
[54] L. Lin, Q. Zhu, A.W. Xu, Noble-metal-free Fe-N/C catalyst for highly efficient oxygen reduction reaction under both alkaline and acidic conditions, J. Am. Chem. Soc. 136 (2014) 11027–11033.
[55] F. Wang, W. Zhang, J. Jiang, J. Xu, Q. Zhai, L. Wei, F. Long, C. Liu, P. Liu, W. Tan, D. He, Nitrogen-rich carbon-supported ultrafine MoC nanoparticles for the hydrotreatment of oleic acid into diesel-like hydrocarbons, Chem. Eng. J. 382 (2020).
[56] Z.-Y. Chen, Y.-N. Li, L.-L. Lei, S.-J. Bao, M.-Q. Wang, H.-L. Heng-Liu, Z.-L. Zhao, M.-w Xu, Investigation of Fe_2N@carbon encapsulated in N-doped graphene-like carbon as a catalyst in sustainable zinc–air batteries, Catal. Sci. Technol. 7 (2017) 5670–5676.
[57] J. Li, F. Yu, M. Wang, Y. Lai, H. Wang, X. Lei, J. Fang, Highly dispersed iron nitride nanoparticles embedded in N doped carbon as a high performance electrocatalyst for oxygen reduction reaction, Int. J. Hydrog. Energy 42 (2017) 2996–3005.
[58] M. Marczewski, E. Kamińska, H. Marczewska, M. Godek, G. Rokicki, J. Sokołowski, Catalytic decomposition of polystyrene. The role of acid and basic active centers, Appl. Catal. B: Environ. 129 (2013) 236–246.
[59] X. Mi, B. Gao, X. Tan, M. Xie, C. Gao, Y. Liu, J. Gao, Preparation of iron and nitrogen co-doped carbon material Fe/N-CCM-T for oxygen reduction reaction, Int. J. Hydrog. Energy 46 (2021) 5332–5344.
[60] B.M.E. Chagas, C. Dorado, M.J. Serapiglia, C.A. Mullen, A.A. Boateng, M.A.F. Melo, C.H. Ataíde, Catalytic pyrolysis-GC/MS of Spirulina: Evaluation of a highly proteinaceous biomass source for production of fuels and chemicals, Fuel 179 (2016) 124–134.
[61] N.M. Aljabri, Z. Lai, K.W. Huang, Selective conversion of polystyrene into renewable chemical feedstock under mild conditions, Waste Manag. 78 (2018) 871–879.
[62] A.M. Alexander, J.S. Hargreaves, Alternative catalytic materials: carbides, nitrides, phosphides and amorphous boron alloys, Chem. Soc. Rev. 39 (2010) 4388–4401.
[63] Z. Wei, J. Wang, S. Mao, D. Su, H. Jin, Y. Wang, F. Xu, H. Li, Y. Wang, In situ-generated Co^0-Co_3O_4/N-doped carbon nanotubes hybrids as efficient and chemoselective catalysts for hydrogenation of nitroarenes, ACS Catal. 5 (2015) 4783–4789.
[64] Z. Liu, J. Yu, X. Li, L. Zhang, D. Luo, X. Liu, X. Liu, S. Liu, H. Feng, G. Wu, P. Guo, H. Li, Z. Wang, X.S. Zhao, Facile synthesis of N-doped carbon layer encapsulated

Fe_2N as an efficient catalyst for oxygen reduction reaction, Carbon 127 (2018) 636–642.

[65] J. Wang, J. Jiang, X. Wang, S. Pang, Y. Sun, X. Meng, M. Li, R. Ruan, A. J. Ragauskas, Enhanced BTEX formation via catalytic fast pyrolysis of styrene-butadiene rubber: Comparison of different catalysts, Fuel 278 (2020).

[66] T. Fu, M. Wang, W. Cai, Y. Cui, F. Gao, L. Peng, W. Chen, W. Ding, Acid-resistant catalysis without use of noble metals: carbon nitride with underlying nickel, ACS Catal. 4 (2014) 2536–2543.